Materials and Design 157 (2018) 512–522

Contents lists available at ScienceDirect

Materials and Design

journal homepage: www.elsevier.com/locate/matdes

Effects of thickness specimen on the evaluation of relationship between tensile properties and small punch testing parameters in metallic materials

M.F. Moreno *

División Física de Metales, Centro Atómico Bariloche, Av. Bustillo 9500, 8400 S. C. de Bariloche, Argentina
CONICET, Argentina

HIGHLIGHTS

- SPT correlation factors calculated are dependent of the materials.
- Bottom displacement provides more extended linearity during regime I.
- Plastic energy evaluations provide new criteria to select PY.
- t/100 method is more representative to define the plastic spreading on SPT.

GRAPHICAL ABSTRACT

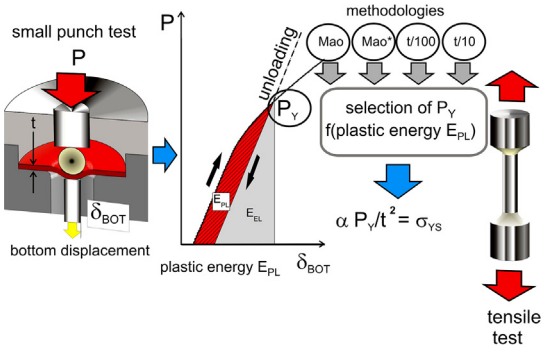

ARTICLE INFO

Article history:
Received 7 June 2018
Received in revised form 16 July 2018
Accepted 31 July 2018
Available online 06 August 2018

Keywords:
Small punch test
Young modulus
Yield strength
Characteristic load
Plastic deformation
Plastic energy

ABSTRACT

The assessment of the yield strength σ_{YS} from characteristic load P_Y obtained from small punch tests (SPT) was studied systematically in aluminum alloys and structural steels by variation in thickness of specimens. Four methodologies of calculating P_Y were considered: Mao and a modification of Mao methods and t/100 and t/10 offset methods. The attempt of correlation between σ_{YS} with P_Y/t^2 by using a unique linear parameter of correlation α was reviewed. Under this framework, it is suggested that the dependence of this correlation factor α with each material cannot be avoided for the four methodologies used to calculate P_Y. The advantage to use the bottom displacement measurement during regime I of deformation is discussed on the assessment of Young modulus and P_Y. Finally, the representativeness of P_Y as the beginning of massive yielding of SPT specimen is also analyzed in terms of plastic energy E_{PL} calculated from SPT plot. Based on the study of E_{PL} evolution during the first regime of deformation, the t/100 offset method resulted the most suitable to select P_Y as characteristic parameter of the beginning of yielding when compared with the other three methods.

1. Introduction

Small punch testing (SPT) has become an interesting technique for mechanical characterization of a wide range of structural and functional materials. Either brittle or ductile behaviors and can be clearly differentiated by SPT among ceramics, composites and metals tested by SPT.

* División Física de Metales, Centro Atómico Bariloche, Av. Bustillo 9500, 8400 S. C. de Bariloche, Argentina.
E-mail address: mmoreno@cab.cnea.gov.ar.

https://doi.org/10.1016/j.matdes.2018.07.065
0264-1275/

[1–8]. The main advantage of this technique is the minimum amount of sample required for manufacturing the specimens (e.g., disks 8 or 10 mm in diameter and 0.500 mm thickness). The size and shape of specimens allow an excellent selectivity of sampling. Thus, several cases employing SPT for mechanical characterization where traditional techniques would be impossible to be employed are found. Just two examples will be mentioned. First, the extraction of SPT disks from already tested standard size Charpy or fracture toughness specimens where the extraction is suitable from undeformed zones. Second, the removal without compromising service conditions of small flakes of material from components using some special tools [9,10]. Under those conditions SPT testing becomes a non-destructive technique. All these advantages over traditional testing techniques, which need relatively larger specimens, have positioned SPT as a potential technique for the study of nuclear materials. In this field the reducing mass of irradiated material becomes critical. Therefore the SPT has been selected as a serious candidate to be applied in hot cells [11] within the framework of surveillance programs. The aim of these programs is to characterize the degradation of irradiated structural component from nuclear plants respect to virgin material. In OPAL nuclear research reactor [12] SPT specimens 6 mm diameter were located to monitor the core reactor materials to guarantee that the surveillance of their mechanical properties are sufficient to ensure safe and reliable long-term operation. The extraction of samples was scheduled for 5, 10, 20, 30 and 40 years of full power operation.

Nowadays, the demand to know the remaining life of power plant has become of fundamental importance to industry, searching for life extension by the applying the monitoring programs [11,13], of critical components under service. In light of this philosophy, the testing by SPT has been proposed to know the level of ageing of material.

Like tensile properties, other important properties as fracture toughness [4,14] or creep strength [15,16] have been studied using SPT by the direct extraction of parameters from a load vs. displacement response (P vs. δ) derived from the test. Within all those applications of SPT is not straightforward the obtaining mechanical properties directly from SPT results. The reason is the complex state of stresses developed during the punching of the disk along the whole test; mixture of elastoplastic processes like indentation, elastic and plastic bending and stretching take place depending on puncher displacement and location into the disk specimen. To solve this obstacle some attempts of interpretation has been proposed. Semi-empirical correlations between particular values taken from P vs. δ curves of SPT and the results of standardized tensile tests were made. Although, important efforts in modeling by the finite elements, including other authors [1,17] and own [3] has been employed, this work is focused mainly in the extraction and interpretation of mechanical properties through experimental data.

In order to standardize the technique, important efforts have been made starting from the CEN Workshop Agreement [10]. This document defines the baselines for the implementation and the interpretation of the SPT results for both room temperature (RT) and high temperatures (creep). In this issue it must be considered the later advances to transform into an EN standard, they can be found summarized in the work of Matocha and Hurst [18]. Concerning RT testing a detailed guide for apparatus manufacturing, specimen preparation, test procedure and interpretation of the results are given in [10].

Typical P vs. δ curve for ductile materials up to maximum load (P_{MAX}) at RT defines regimes of deformations, which have been arbitrarily classified [1,4,17,19]. In search to define how the elastic bending stresses reach the yield strength σ_{YS}, singular points (or regions) of SPT curve have been identified. The most relevant feature is the transition between the two first regimes of deformation: the so called elastic bending (regime I) and the plastic bending (regime II). The characteristic load P_Y has been widely used as the representative parameter for this change. Under this point of view some authors [8,20–23] have established directly P_Y as the equivalent in SPT to yield strength σ_{YS} obtained in uniaxial tensile test. This type of relationship reveals the potential of SPT like a technique for further tensile properties predictions like σ_{YS}, tensile strength σ_{UTS} and other. That is the reason why SPT needs a deeper study and the present work will focus on the semiempirical relation of σ_{YS} proportional to P_Y/t^2 where t is the initial thickness of the specimen. This relation, adopted initially by Mao and Takahashi [20], has been followed by many authors [4,6,19,23,24]. The proportional factor between σ_{YS} and P_Y/t^2 is α, also known as the correlation parameter. Focusing on σ_{YS} assessment, a detailed analysis reveals that there are many proposed methodologies to define P_Y [3,4,8,17] for a single material. Of course, this leads to many α for each material depending on which definition of P_Y is adopted. Only few specific works have systematically studied the physical meaning of P_Y for each one of these methods. In the work of reference [3] the level of volume under plastic regime and the stresses distribution reached at P_Y it has been thoroughly studied. SPT specimens of 10 mm in diameter and 0.5 mm in thickness made from AISI304L stainless steel were tested and such results were modeled by finite elements (FEM).

The influence on the selection of the P_Y, among four definitions, and its correlation between σ_{YS} and α is systematically studied as a continuation of the previous work [3]. For that purpose ductile alloys such as structural steels and Al alloys have been employed to analyze their mechanical behavior by SPT and their relationship with the properties obtained from the corresponding uniaxial tensile tests. As a consequence, an important issue to be discussed is the level of dependence of α with different materials. This parameter has been proposed as `universal´ proportionality factor between σ_{YS} and P_Y/t^2 independent of material [4,8,20,23]. Here, the proposed material independence was thoroughly revised.

Finally, the significance P_Y calculated by four methods were evaluated in terms of plastic energy obtained from experimental P vs. δ curve. The evolution of this parameter plays an important role in the interpretation of the plastic process at P_Y. Thus a new method to select P_Y as the most representative of yielding is introduced.

2. Experimental

2.1. Materials

The materials used in the present study can be arbitrary separated in two groups: Al based materials and structural steels. They were selected by the wide range of mechanical strengths and ductilities; and also they are representative of materials for nuclear, laboratory and structural applications. Denominations and details of materials are given in Table 1. AISI 304 L stainless steel and heat resistant high Cr P91 steel belong to

Table 1
Materials used for the present study.

Denomination	Al	Aluar	AlZn	6061	304	P91	ADN
Material	Al 99.99999	Al 99.5	AlZn11Mg0.5	6061-T6	AISI304L	ASTM A335 grade P91	ADN420
Provider	Chempur, Germany	Aluar, Argentina	Alusuisse-Lonza	Alcoa, US	n/a	JFE Steel Corporation, Japan	Acindar, Argentina [25]
Shape	10 mm cylindric bar	Ingot	Squeezed cast block of 20 mm	12 mm bar	12 mm cold drawn bar	Pipe of 355.6 mm in diameter and 28 mm in thickness	32 mm bar

materials studied in references [3,19] respectively. ADN is a kind of steel widely used as reinforce bars [25] in concrete, also known as 'rebar'. Aluar is a commercially pure ingot Al and 6061 is the commercial heat-treatable high strength aluminum alloy with T6 temper. AlZn corresponds to unreinforced part of synthetized composite material by squeeze casting. Details of composite manufacturing can be found in the reference [26].

2.2. Tensile tests

The tensile properties of the materials were obtained through uniaxial tensile tests performed at RT. All materials, excepting AlZn were standard specimens of cylindrical shape. They were machined and polished. AlZn was cut as plate specimen by a spark erosion and metallographic saw and finally polished up to 1200 grit emery paper. Tensile tests of steels were performed using a servohydraulic MTS 810 testing machine. The first part of the tensile test was monitored by an extensometer MTS 632.12C-20 with a gauge length of 10 mm. Uniaxial tests of aluminum materials were performed in an electromechanical Instron 5567 testing machine. The first part of the tensile test was monitored by an extensometer MTS 632.13F-20 with a gauge length of 25 mm. The initial strain rates adopted during tensile tests are listed in Table 2.

2.3. Small punch tests

Disks shaped specimens 10 mm in diameter were used for SPT. The adopted thicknesses for systematic studies were 0.400, 0.500 and 0.600 mm with a thickness tolerance of about ±1%. Due to the importance of thickness measurements one micron resolution micrometer was used. Five points were covered to measure the thickness: one located on the center and the rest over four points randomly located near to the circumferential edge. In certain cases other thicknesses were employed (e.g. 0.700 or 0.350 mm). The details of specimen preparation, apparatus used for testing, including the displacements measurements systems were thoroughly described elsewhere [3,19]. Concerning SPT apparatus some recommendations from the European Code of Practice [10] has been followed. The diameter adopted in this work was 10 mm, while 8 mm is recommended by CEN.

In order to avoid any confusion it is very important to differentiate between four specific displacements regarding to SPT test: i- δ_N is the imposed by crosshead testing machine; ii- δ_{EXT} measures the plunger movement (that pushes the indenter ball) by an extensometer MTS 632.13F-20 attached to upper die [3], iii- δ_{TOP}, the displacement of contact point between the ball and the punched face of disk, which results from the subtraction from δ_{EXT} of the displacement due to the compliance of the plunger and ball together; and, iiii- δ_{BOT} is the displacement of opposite side to contact ball face and it was measured directly by a contact rode connected to a displacement transducer HBM W1 T3 [3].

In all cases crosshead speed δ_N/dt of 0.1 mm/min were controlled by Instron 5567 testing machine during SPT.

Several SPT were conducted in this study: first, it was made an evaluation of general P vs. δ_{BOT} behavior beyond P_{MAX} up to rupture. Then, tests for all materials were conducted up to P_{MAX} followed by total unloading.

Table 2
Materials and tensile properties derived from uniaxial tensile tests of Fig. 1. (*) calculated at upper yield point (UYP).

	E [GPa]	σ_{YS} [MPa]	σ_{UTS} [MPa]	ε_U [mm/mm]	$\dot{\varepsilon}_0$ [1/s]
304	210	652	820	0.26	1.2×10^{-4}
P91	213	512	666	0.09	5.0×10^{-4}
ADN	218	454*	668	0.15	1.0×10^{-3}
Al	66	18	36	0.38	1.0×10^{-4}
Aluar	67	25.4	51	0.22	1.0×10^{-4}
AlZn	69	215	243	0.03	1.0×10^{-3}
6061	70	330	372	0.08	1.1×10^{-3}

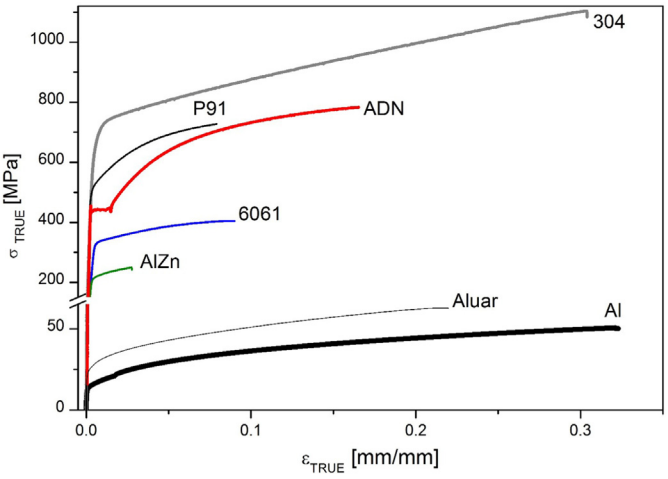

Fig. 1. Uniaxial tensile tests of all materials.

At least three tests of 0.500 mm thickness specimens up to P_{MAX} were performed for all materials to evaluate the reproducibility of the experimental results.

3. Results and discussion

3.1. Uniaxial tension behavior

Fig. 1 shows the plots of the true stresses as a function of the true strains obtained during tensile tests. 304 [3] and P91 [19] steels showed work hardening behavior with high and middle elongation range respectively. ADN steel showed a characteristic upper yield point (UYP), followed by a sudden drop of tension and a sequence of constant stress and finally an increase of stress due to hardening typically found in low-carbon structural steels.

Also in Fig. 1 it can be seen that Al materials selected had completely different tensile behaviors in terms of strength. Poor mechanical strength and high ductility for Al and Aluar were observed. In contrast, for 6061 and AlZn, relative high strengths and limited ductilities were observed. The tensile properties obtained for all materials are given in the Table 2. Excepting for ADN, the yield strength σ_{YS} corresponding to the rest materials were defined at 0.2% offset engineering strain. The ultimate tensile strength σ_{UTS} and the elongation strain ε_U up to σ_{UTS} are also listed in Table 1.

3.2. Small punch tests

3.2.1. P vs. δ_{BOT} behavior until P_{MAX}

In reference [3] it was discussed the importance of distinguishing between two displacements that can be assessed from specimen center during a SPT test: δ_{TOP} and the opposite side δ_{BOT}. Cited work details the advantage to use δ_{BOT} due to that reading results from a direct measurement (without need of any correction discount). Thus δ_{BOT} is not affected by compliance effects of load train (e.g. plunger plus ball or puncher). Concerning the P vs. δ_{BOT} behavior, this reading provides more extended range of linear response during the regime I of elastic bending when is compared with δ_{TOP}. This feature was previously observed for both steels 304 [3] and P91 [19], and it was systematically repeated for all tests in the rest of materials. Regarding CEN [10] definitions, deflection and punch displacement were established equivalent to δ_{EXT} and δ_{BOT} in this work respectively. However, punch displacement is recommended by CEN to calculate the characteristic load P_Y.

For further discussions, the most of results in the present work will be represented in terms of P vs. δ_{BOT}, excepting in the subsection dedicated to discuss the regime I. Fig. 2a to c show the plots P vs. δ_{BOT} for the three steels tested on 0.400, 0.500 and 0.600 mm specimens

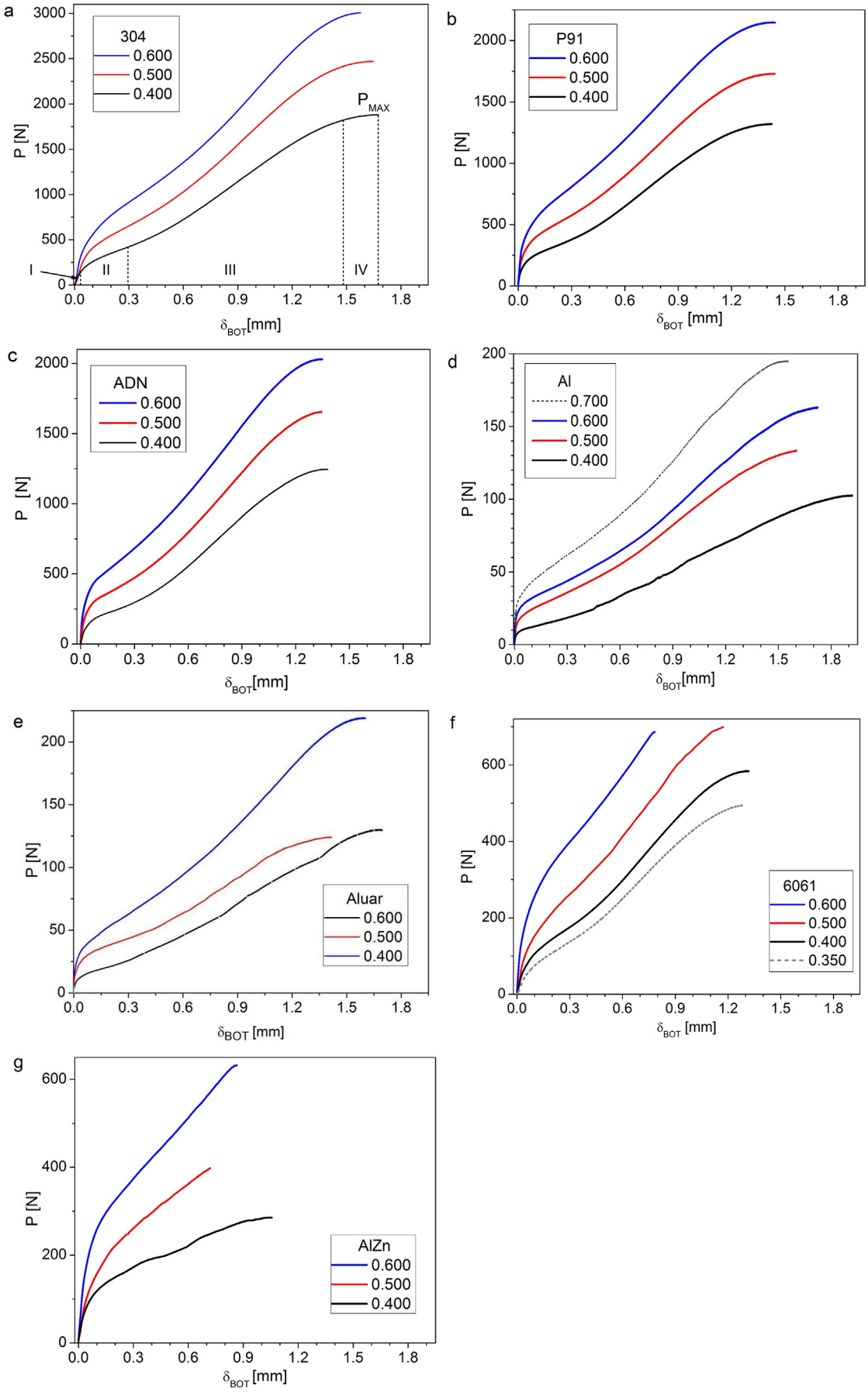

Fig. 2. (a to g) Experimental P vs. δ_{BOT} plots until P_{MAX} for all materials. Test of 0.700 mm specimen is included for Al (d) and test of 0.350 mm specimen is included for 6061 (f).

respectively, up to P_{MAX}. These plots represent clearly the arbitrary regimens of deformations typically found in work hardening ductile materials [3,4,19,20]: I- elastic bending, II- plastic bending, III- membrane stretching and IV- plastic instability before reaching P_{MAX} (see detailed classification separated by dashed lines in 0.400 mm thick plot of Fig. 2a). A good reproducibility for the three steels among the tests of specimens of 0.500 mm thickness was achieved, thus for plots of 0.500 mm in Fig. 2a, b and c are representative of several tests. Also for pure aluminum (Al and Aluar) regimens I, II, III and IV were observed. However, for 6061 and AlZn the deformation only covered the regimes I and II before to achieve the rupture due to low ductility.

3.2.2. Thickness effects on P vs. δ curve

Relative scatter works dedicated by experimental methods to systematic study the thickness effects on SPT behavior are found. Most of them perform analyzes this topic mainly modeling by FEM. In the present work all tested materials by SPT showed clearly an increase of load with thickness. 304, P91 and ADN steels showed a systematic load increase with thickness, observed along the whole tests plots in Fig. 2a, b and c. The load increment referenced to 0.500 mm thickness specimen test has been proposed as proportional to 0.5/t during regime II and III according to proposed by Cuesta [6]. Applying this dependence, only satisfactory agreement for the three steels 304, P91 and ADN were found, mainly because of well-defined curves representative of four 'typical regimens of deformations' for all thicknesses.

Some authors have related δ_{MAX} and P_{MAX} with ε_{UTS} and σ_{UTS} respectively [4,24,27]. However, recently recent interpretations [8,28] suggested that other parameters should be computed from SPT considering whether or not damage is developed. In contrast with deformation state at σ_{UTS} in tensile test, P_{MAX} has reached the maximum capacity to stand load in SPT, beyond this point load start to fall until fracture. In addition, small cracks or surficial voids were detected in all specimens of the present work at P_{MAX} according to SEM and optical observations, therefore the damage has started at lower loads than P_{MAX}.

Fig. 2f and g shows the SPT behavior for 6061and AlZn respectively. For 0.600 mm thick specimen of 6061 regime III (membrane stretching) is restricted due to a sudden appearing of P_{MAX}, followed by fracture. This anticipated break, reduces significantly δ_{MAX} when it is compared with those ones for thinner specimens. For thicknesses 0.400 and 0.350 mm, the curves recovered the well-defined shape of four regimens (similar that found for Al and steels). As the same way, the separation between regimens II and III defined by the inflexion point becomes more defined. The reduction of thickness/diameter specimen ratio allows extend the regime III according to discussed by of Eskner [22]. This effect can be observed in Fig. 2f for 6061 as the thickness decreases.

The regime III is very hard to identify in AlZn as it is shown in Fig. 2g. After slope change to regimen II, the deformation extended until δ_{MAX} followed by a sudden rupture. After repeat SPT tests for same thickness δ_{MAX} resulted into wide scatter low values (0.5–0.8 mm). This behavior can be associated to limited ductility observed in tensile test (Fig. 1).

3.2.3. Regime I

The set of plots showed in Fig. 3a summarizes the regime I of deformation corresponding to 0.500 mm thick specimens. The most relevant feature is the linear behavior of P vs. δ_{BOT} [3] obtained for all tests. This represents mainly the elastic stiffness response unambiguously captured by displacement δ_{BOT}. Due to poor mechanical properties of Al and Aluar, the extension of regime I covered only few microns.

In order to evaluate this behavior, partial or total unloadings (UL) were performed during this regime for all materials. Examples of UL for ADN and 6061 are shown in Fig. 3b, where cycle paths (indicated by arrows) resulted straight linear and coincident with the same slope of loading when δ_{BOT} is employed.

The second observation during regime I is the clear distinguishing between the slopes ($S_{BOT} = \Delta P/\Delta\delta_{BOT}$) belonging to steels and Al alloys (Fig. 3a). The assessing of the Young modulus E can be done for clamped or unclamped punched disks by performing linear fittings of S_{BOT} [29]. For same thickness, the ratio $S_{BOT}^{(steel)}/S_{BOT}^{(Al)}$ is close to 3, in agreement with ratio between E for carbon steel and 6061 (218GPa/70GPa). Until now, the sensitiveness of SPT to capture the incidence of E has paid attention mainly to be simulated by FEM [1]. Such work indicates the strong influence of E over S_{BOT} during regime I. It must be pointed out that according to tests performed in this work the sensitiveness becomes more evident when the bottom measurement δ_{BOT} was employed. Otherwise, if the top measurement δ_{TOP} would be included, a not negligible amount of plastic indentation is captured. Whether or not hard materials, plastic indentation always takes place at very low loads during SPT. Such indentations were found in both steels and Al materials, after UL during regime I followed by SEM and optical observations on punched faces.

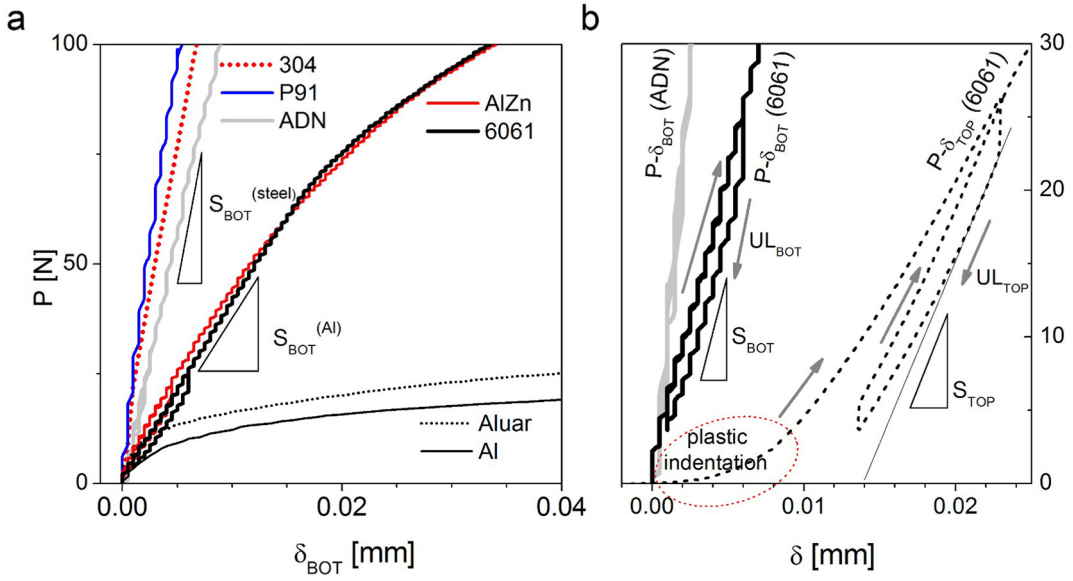

Fig. 3. (a) Regimes I and II of SPT tests for all materials corresponding to 0.500 mm thickness specimens. (b) Low loads range of ADN and 6061 tests from Fig. 5(a). P vs. δ_{BOT} plot is also included for 6061 showing UL path.

Looking for comparative characterization, P vs. δ_{TOP} during both previous studies [3,19] and present work was also evaluated. The main findings were systematically repeated and can be listed as: i- no reversible behavior and lack of linearity or very short range of linear behavior of P vs. δ_{TOP} were found during loading path; ii- slopes during UL (S_{TOP}) were higher than S_{TOP} calculated during loading; and, iii- S_{TOP} during UL were 15–20% lower than S_{BOT} obtained with P vs. δ_{BOT}. Last three features are shown in Fig. 3b for 6061 in a specimen of 0.500 mm. Essentially δ_{TOP} is representative of tip puncher movement (or ball) and it is extremely difficult to read directly the linear displacement of this point. Corrections were made by punching over a hard tungsten carbide specimen to know the compliance of loading system. After discount, still it is extremely difficult to separate the pure specimen displacement on the top face from the contribution of elastic compliance and contacts from loading kinematic chain. Recent efforts has been carried on this issue for other researchers [17] looking for a distinguishing the displacement (or deflection) component attributed to bending from those coming from elastic indentation and shear stresses as a function of δ_{TOP}.

Taking attention only in the bending deflection for an elastic thin plate in a clamped punched disk, E can be expressed as a function of S_{BOT} [29] in the following form:

$$E = S_{BOT} 3\, R^2 (1-\nu^2)/(4\pi t^3) \quad (1)$$

where R is the receiving hole radius (2.5 mm for the adopted configuration) and ν the Poison coefficient. Accurate experiments in brittle disk specimens have shown that this expression is a good prediction of E using δ_{BOT} [29]. The application of Eq. (1) gave values of E of about 145,000 to 180,000 MPa and 45,000 to 50,000 MPa for steel and Al alloys respectively, which represent between 65 and 85% of expected modulus. Eq. (1) considers that puncher diameter remains constant during punching and this is not the actual condition in SPT, especially during regime I. Even considering the contact diameter variation with applied load similar lower values of E were still found. The underestimated results of applying expression (1) mean that the experimental deflection δ_{BOT} is higher than expected for a pure membrane deflection under pure elastic bending, thus a lower S_{BOT} is captured by experimental data during regime I. As it was discussed previously the plastic deformation cannot be avoided during regime I over the top face specimen. Thus, the effective S_{BOT} represents the deflection coming from bending, and it should incorporate other contributions from top face, like elastic and plastic indentations and shear stresses. The contribution of pure elastic indentation and shear strain has been studied by [17] based on δ_{TOP} measurements. It must be pointed out that for all materials tested in the present work S_{BOT} is about 15–20% higher than the highest value of S_{TOP}, therefore S_{BOT} is more representative to be related with E. Last advantage should be evaluated previously to setup of SPT experiments if regime I will be considered to evaluate the elastic modulus.

In addition to previous findings, S_{BOT} is also strongly affected by thickness due to change of geometrical stiffness. Variation of S_{BOT} with thickness can be seen in Fig. 4a, and b for ADN and 6061, respectively. Regarding the limitations of expression (1), the incidence of thickness can be expressed fitting of S_{BOT} as a function of t^3. Satisfactory agreements for S_{BOT} and thicknesses taken from Fig. 4a and b were found. According to linearity and ratio between both slopes (110,100 and 37,876) it was reproduced the ratio $E^{(steel)}/E^{(Al)}$~3.

3.2.4. Characteristic load P_Y

In order to extract σ_Y from the mechanical response of SPT the characteristic load P_Y has been extensively used. The well-known relationship is that one adopted by Mao and Takahashi [20] based on a clamped thin plate subjected to axis-symmetrical load:

$$\sigma_{YS} = \alpha P_Y / t^2 \quad (2)$$

where α is the correlation parameter and t is the initial thickness.

The elastic-plastic transition from regime I to II is represented by P_Y [3,4,24], which is often associated with the deviation from linearity of P vs. δ_{BOT} plot, that is, the end of regime I of 'elastic bending'. As mentioned above, small volume of plasticity due to plastic indentations is found from early low loads at the beginning of regime I [3,11]. However the linearity of P vs. δ_{BOT} remains constant along load increase until that yielding reach level enough to spread across the thickness [3]. It that condition, P_Y is assumed as representative of beginning of massive yielding. The most important concept to point out is that there is no sudden transition from pure elastic to plastic regime in SPT. Thus, the debate is focused on how to select the proper P_Y due to that several criteria have been proposed. Mao and Takahashi [20] defined P_Y, called $P_Y{}^{MAO}$ in the present work, as the intersection between the two representative fitting straight lines of regimes I and II. As an alternative to this method in the reference [3] it was proposed to define P_Y^{MAO*} as the value that fall over P vs. δ plot. P_Y^{MAO*} can be considered like more realistic load associated with the plastic behavior than P_Y^{MAO}. Other methodologies based on offset criteria like $P_Y{}^{t100}$ and $P_Y{}^{t10}$ can be found [4] as well. They resulted from the intersections of offset parallel lines to regime I arbitrary shifted a displacement t/100 and t/10 respectively. Unlike

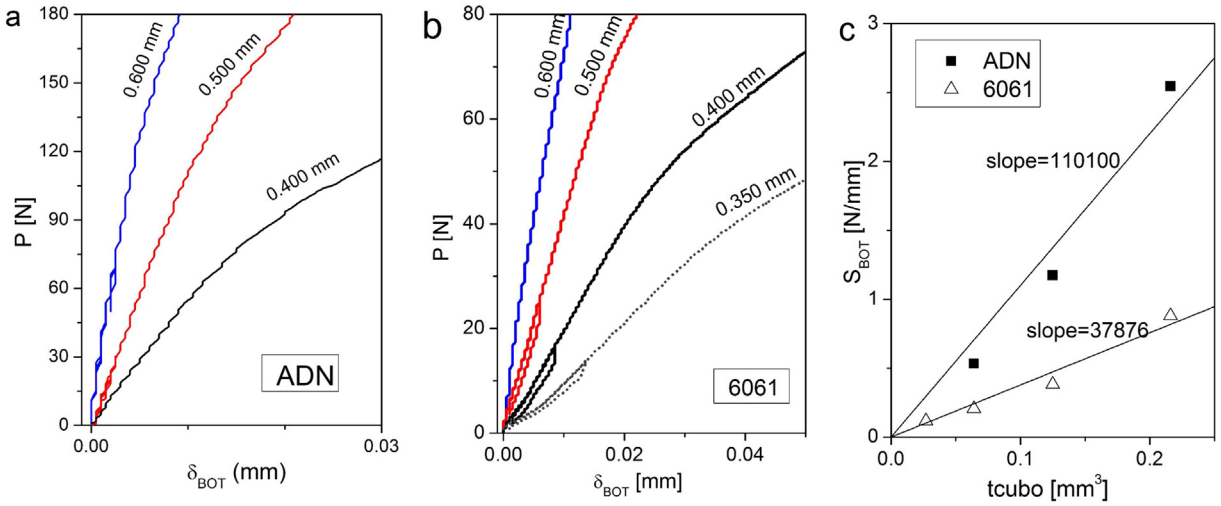

Fig. 4. Regimes I for tests of (a) ADN and (b) 6061. (c) Linear fittings of S_{BOT} obtained from Fig. 6a and b using Eq. (1).

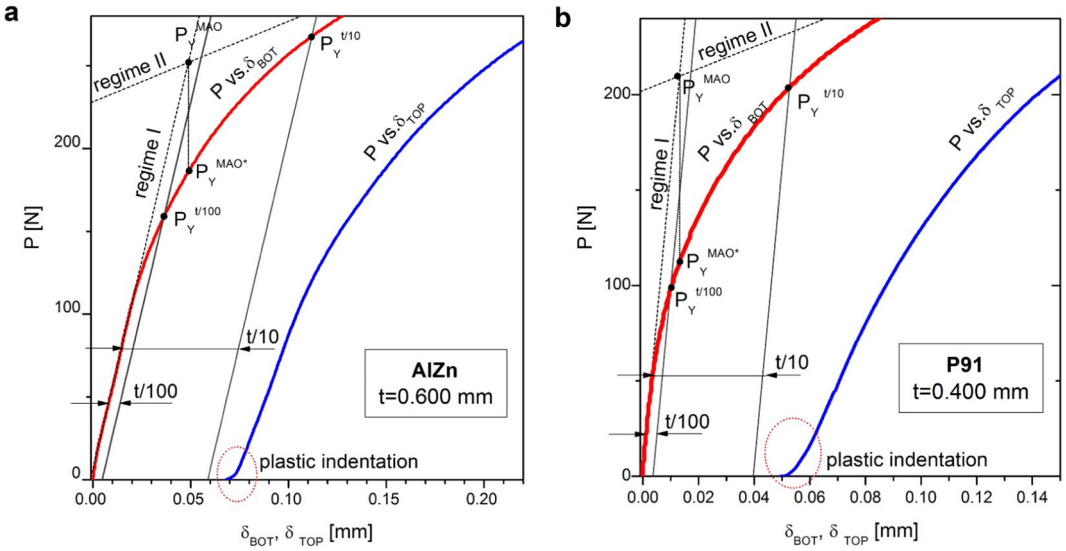

Fig. 5. Definitions of characteristic loads P_Y using P vs. δ_{BOT} plots for (a) 0.600 mm thick specimen of AlZn and (b) 0.400 mm thick specimen of P91.

P_Y^{MAO} and P_Y^{MAO*}, both methods need only the slope of regime I to be applied. Other criteria, including the definition of P_Y by CEN [10] are summarized in the work of [8]. The definitions of P_Y that will be systematically studied in the present work are: P_Y^{MAO}, P_Y^{MAO*}, P_Y^{t100} and P_Y^{t10}.

Examples of characteristic loads defined by the four methodologies are showed in Fig. 5a and b in terms of P vs. δ_{BOT} (0.600 and 0.400 mm specimens of AlZn and P91 specimens respectively). Also plot of P vs. δ_{TOP} has been included in both figures, showing of plastic indentation at the beginning and the reduced range of linearity during regime I.

3.2.5. Correlation parameter α

Under the hypothesis that (2) is valid for different thicknesses (t), P_Y must accomplish the variation of t to keep constant P_Y/t^2 due to σ_{YS} is a known constant. Then, the values of σ_{YS} t^2 can be fitted by the straight line with their respective P_Y for different thicknesses. According Eq. (2) the slope extracted from this fitting represents α [19]. This relationship was systematically employed for all materials in Fig. 2a to g using the set of P_Y taken from all thicknesses tested. Haroush et al. [30] showed that Eq. (2) applied for specimens of 316 austenitic steel (in square specimens of 8 × 8 mm and thicker than 0.300 mm), are still valid to provide adequate correlation between P_Y and σ_{YS}.

Fig. 6a to g are representative of the linear fittings of σ_{YS}/t^2 vs. P_Y for all materials that belong to this work. For each material the four methods to calculate P_Y^{MAO}, P_Y^{MAO*}, $P_Y{}^{t100}$ and $P_Y{}^{t10}$ were employed using the P vs. δ_{BOT} plots. As result, a set of four correlation parameters α^{Mao}, α^{Mao*}, $\alpha^{t/100}$and $\alpha^{t/10}$ was obtained from the slopes of linear fittings in Figs. 6a to g. It should be noted that regressions were obtained with good fitting, in the worst of case the regression parameter R^2 was about 0.97.

Often it can be found some attempts to find a representative α by linear regressions of σ_{YS} vs. P_Y t^2 for many materials in the same fitting. A comprehensive work for a several metallic materials with a broad range of strengths was made by García et al. [4]. Such approach joined the whole materials around a 'common' α taken as representative to predict yield strengths by Eq. (2). However, limited agreement in linear fittings could be achieved, even using several methodologies including Mao, t/100 and t/10. In a different point of view in this work first it was systematically analyzed the isolated value of α for in each material.

3.2.6. Material dependence of α

The whole collection of correlation parameters α^{Mao}, α^{Mao*}, $\alpha^{t/100}$and $\alpha^{t/10}$ are summarized in Fig. 7a, where they were arbitrary sorted by roughly increasing value. It is noticed that there is a variation of α according each method, but systematically close similar values were found between α^{Mao} and $\alpha^{t/10}$ for all materials. That is consequence of close similar P_Y found between both methods (see definitions of P_Y in Fig. 5a and b).

Concerning absolute values of α^{Mao} only the three steels were in good agreement with the correlation factor $\alpha^{Mao} = 0.36$ predicted by Mao and Takahashi [20] (dashed line in Fig. 7a). However α^{Mao} for Al, Aluar and AlZn were under 0.36, and in contrast 6061 alloy resulted with the highest α^{Mao} close to 0.5.

The strongest material dependence and broad variations among nominal values of $\alpha^{t/100}$ could be observed. The highest variation was more than twice from Al ($\alpha^{t/100} = 0.39$) to 6061 ($\alpha^{t/100} = 0.99$). The interest on t/100 method is focused on the representativeness of beginning of yielding during regime I. In detail, according to study by FEM in 304 [3] the $P_Y{}^{t/100}$ is coincident with the complete spreading of plastic regime across the whole thickness specimen.

Fig. 2a to g showed the extreme levels of loads depending on mechanical strength of each material in terms of P vs. δ_{BOT}. In Fig. 7b altogether materials were plotted as a function of δ_{BOT} normalizing P by (t^2/σ_{YS}). The transition between regimes I and II for 0.500 mm thick specimens are showed in detail. As a consequence, plots get together in separated groups: i- Al and Aluar, ii- steels and AlZn, and iii- 6061. From Eq. (2) normalized load P t^2/σ_{YS} represents $1/\alpha$ when $P = P_Y$ over y-axis for any method (Fig. 6b). This procedure revealed that different values of α as can be seen for Al, 304 and 6061 by using t/100 method. Thus, the joining of 'arbitrary' groups of normalized load indicates as a rough way that the correlation parameter α is strongly material dependent as it was established previously in Fig. 7a. Finally, concerning to material dependence it can be suggested that microstructural parameters (e.g. that grain size [27] or strengthening mechanisms) could be responsible for such segregation in groups but more work is need in this sense to study both, the parameters that affect this classification and the importance of such dependence.

3.2.7. P-δ_{BOT} behavior for UYP material

When the three steels ADN, P91 and 304 SPT plots of Fig. 2a, b and c, and in detail Fig. 7b are examined, similar curvatures are observed during transition from regimen I to II. That indicates a drastic change of yielding behavior under multi-axial stresses state due to SPT. While a well-defined UYP is observed under uniaxial stress of ADN steel (Fig. 1), it seems that SPT conditions hinder typical Lüdders

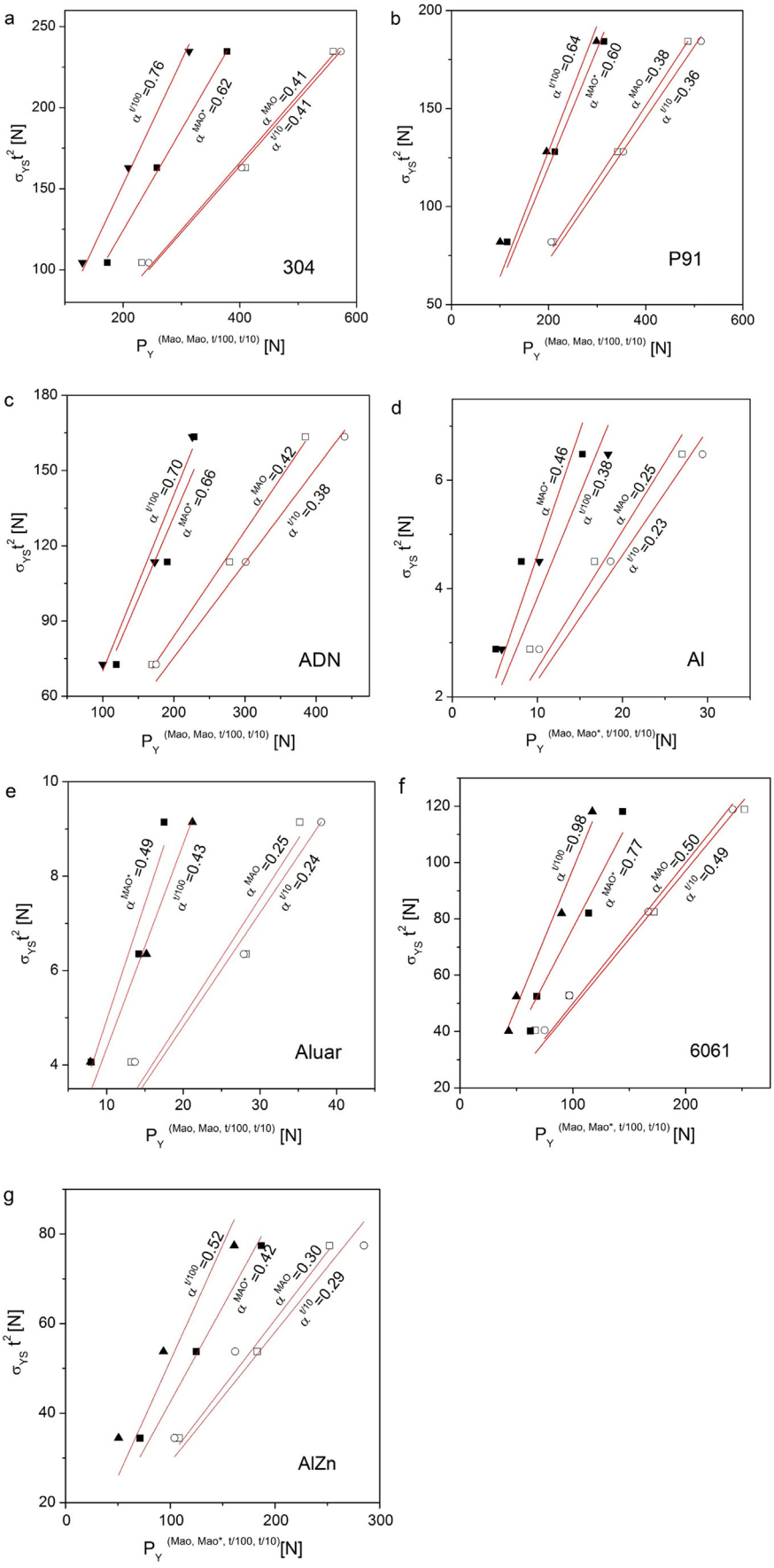

Fig. 6. Linear fittings for determining the correlation parameters of (a) 304, (b) P91, (c) ADN, (d) Al (0.700 mm thick specimen were also included), (e) Aluar, (f) 6061 (0.350 mm thick specimen were also included), and (g) AlZn.

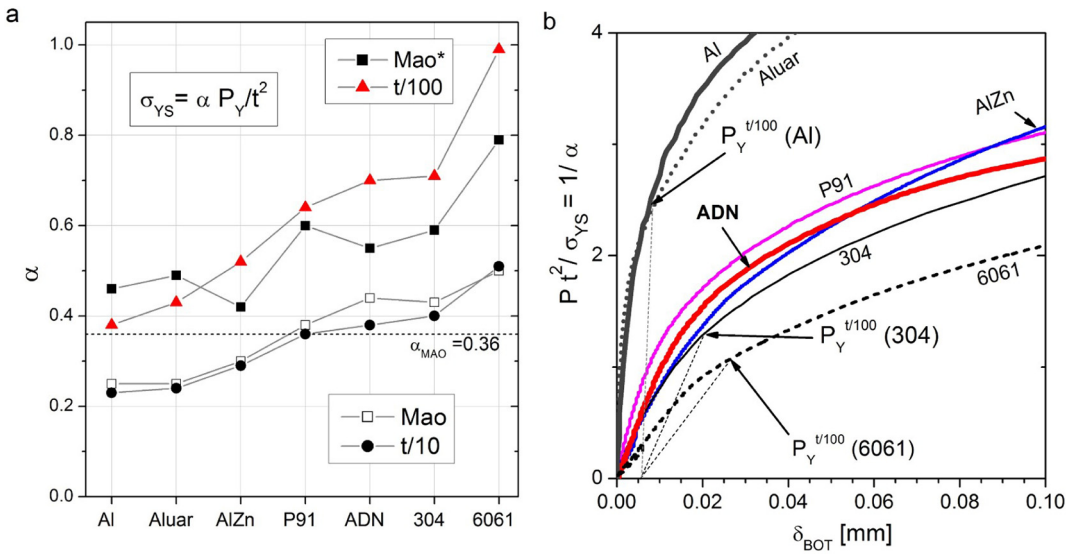

Fig. 7. (a) Correlation parameters α obtained from Fig. 6a to g by Mao, Mao*, t/100 and t/10 methods for all materials. (b) Normalized load vs. δ_{BOT} for specimens of 0.500 mm thickness.

bands mechanism. After indentation a progressive spreading of non-homogeneous stresses is reached and the plasticity takes place across the thickness during transition from regime I to follow regime II. In contrast during uniaxial test (Fig. 1) the thinned length of tensile specimen that reaches the end of elastic regime is subjected to homogeneous stress at the same time. This feature reveals that ADN steel deforms continuously during regime I of SPT reaching the full plastic regime without any sudden change or unstable process (there is no equivalent to UYP in SPT) developing similar deformation mode like work-hardening steels P91 or 304.

3.2.8. Evolution of plastic energy until P_Y

Many SPT studies have focused on the discussion which methodology is the most representative to relate P_Y with σ_{YS} based on the accurate prediction of correlation factor. From Section 3.2.6 it was established that the correlation factor has different levels of dependence with material as a function of methods to calculate P_Y. From this fact, it must be pointed out the need of physical interpretation of deformation under SPT at P_Y. Therefore, for the proper understanding of mechanical process, based on experimental SPT data, a plastic parameter must be selected. Thus, a new method to evaluate the mechanical energy along regime I until P_Y will be introduced.

The area under SPT plot (applied load by the puncher displacement) represents the total mechanical energy (E_{TOT}) applied to the specimen and can be expressed as the sum of the elastic and plastic mechanical energies, E_{EL} and E_{PL} respectively (Fig. 8a). As it was mentioned above indentation marks after interrupted tests during regimen I and the non-linear beginning of P vs. δ_{TOP} plot indicate that plastic indentation is developed early at very low loads, even for hard materials, like 304 steel. Thus, the E_{TOT} represents an important plastic fraction belonging to indentation. Performing same analysis in terms of P vs. δ_{BOT} the dominance of elastic behavior during regime I can be clearly detected first (Fig. 8b). Thus, it is possible to identify the transition to plastic regime due to the plasticity reaches the bottom face after crossing completely the thickness disk [3]. For that purpose, first E_{EL} is computed from the area under the straight line defined by the slope of unloading in accordance to scheme of Fig. 8a. Finally, to calculate E_{PL}, E_{EL} is subtracted from E_{TOT}. The appearing of sudden increases and law of increment of E_{PL} can be studied as a function of δ_{BOT}. This procedure was applied during the regime I and initial part of regime II and multiple unloadings during both regimes were useful to accurately follow this approach. Evolutions of E_{TOT}, E_{PL} and E_{EL} were plotted in Fig. 8b for 304 asa function of δ_{BOT}. It can be seen that the level of E_{PL} after a delay, started to raise until represent the biggest fraction of E_{TOT} with δ_{BOT} progress. Same

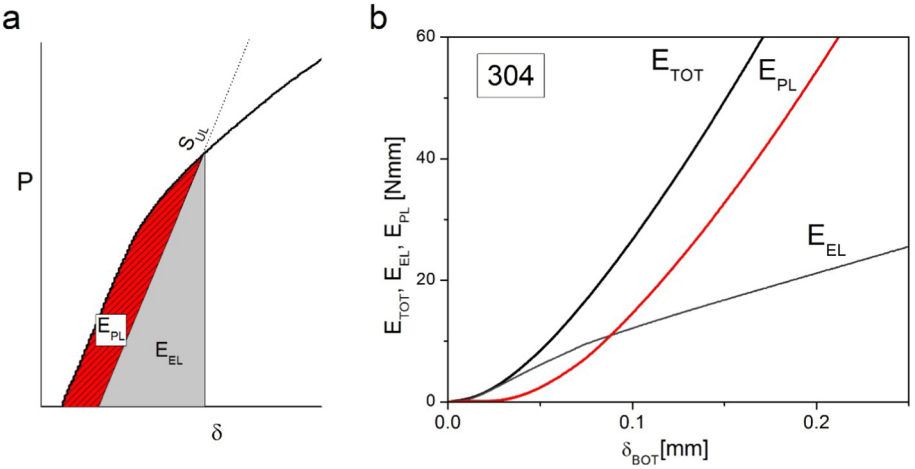

Fig. 8. (a) Scheme of calculation of E_{EL} and E_{PL} computed from P vs. δ, E_{EL} is the elastic energy defined by the slope of unloading (S_{UL}). (b) Evolutions of E_{TOT}, E_{EL} and E_{PL} as a function of δ_{BOT} for 0.500 thick specimen of 304.

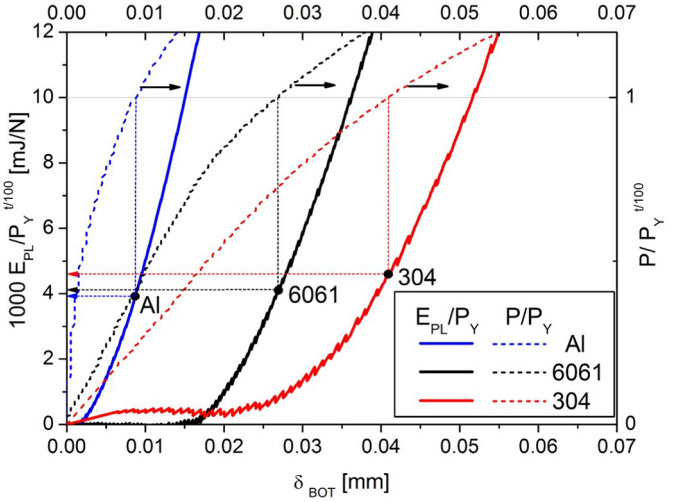

Fig. 9. Evolutions of normalized E_{PL}/P_Y (left axis) and load P/P_Y (right axis) for method t/100.

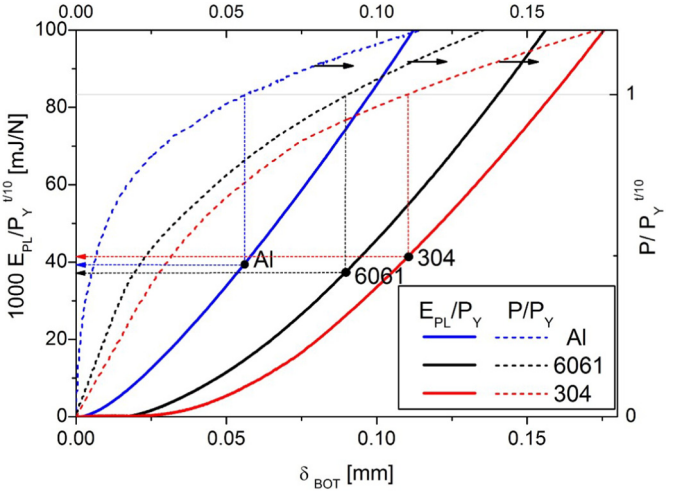

Fig. 11. Evolutions of normalized E_{PL}/P_Y (left axis) and load P/P_Y (right axis) for method t/10.

behavior was determined in 304 for plastic deformed volume as a function of δ_{BOT} of 304 calculated by FEM in [3]. Besides 304, Al and 6061 were selected to be also analyzed under this framework. These materials represent both, the widest extreme mechanical strengths (Al and 304) and the widest range of α (Al and 6061, Fig. 7a). Only t/100, Mao* and t/10 methods were considered for comparison purposes, due to Mao defines P_Y out of P vs. δ curve, and the nominal value for this characteristic load is similar to that obtained for t/10 method.

Paying attention to broad range of loads during SPT the nominal values of E_{PL} extracted from P vs. δ_{BOT} plots fall in different orders of magnitude depending on the material. A kind of normalization of E_{PL} by respective $P_Y^{t/100}$ was made for Al, 6061 and 304 to represent E_{PL} under the same scale as a function of δ_{BOT} in Fig. 9 referenced to left axis. Same 'normalization' $P/P_Y^{t/100}$ was made for loads and their respective plots referenced to right axis are shown in Fig. 9 as a function of δ_{BOT} also. On the one hand the delay mentioned above for 304 is repeated in Fig. 9 for normalized energies (see referenced to left axis), on the other hand shorter and almost negligible delays are found for 6061 an Al respectively.

Then, evaluating $E_{PL}/P_Y^{t/100}$ at $P_Y^{t/100}$ (see vertical dashed lines in Fig. 9), that means at $P/P_Y^{t/100} = 1$ referenced to right axis, values of 0.0036, 0.0041 and 0.0045 mJ/N are obtained. They are indicated on left axis for Al and 304 and 6061 respectively, which represent in average close similar results. In Fig. 10 latter comparison was made for Mao* method, that is normalize by $P^{Mao*b}E_{PL}$ and P. After evaluation at $P/P^{Mao*} = 1$ wide difference was obtained between E_{PL}/P^{Mao*}: 0.002, 0.0116 and 0.0318 mJ/N for Al, 6061 and 304 respectively. Finally Fig. 11 shows that for t/10 method $E_{PL}/P_Y^{t/10}$ gave values of 0.039, 0.038 and 0.041 mJ/N for Al, 6061 and 304 respectively at $P/P^{t/10} = 1$. All results of E_{PL}/P_Y are summarized in Fig. 12 and it can be observed that t/100 allows for Al, 6061 and 304 the lowest values respect to other methods with almost negligible variation. In contrast for Mao* the variation of E_{PL}/P_Y^{Mao*} is noticeable reaching a thirteen times higher for 304 respect to Al. Finally, for t/10 method the calculated values are into a reasonable low variation between three materials, but the level of $E_{PL}/P_Y^{t/10}$ is about one magnitude order over $E_{PL}/P_Y^{t/100}$ results. This ratio is in trend to that obtained from volumes of material under plastic regime calculated by FEM for 304 in reference [3] for same methods.

Based on good linear fitting of σ_{YS} vs. $P_Y^{t/10}/t^2$ on the one hand and due to fully plastic regime has reached at this level of deformation on the other hand, some authors [4,24] argued that t/10 offset method is more representative to select P_Y. According the level of deformation calculated in [3] and the comparative analysis from the present work the plasticity that cross through the thickness specimen has been reached by far before $P_Y^{t/10}$. The bottom displacement δ_{BOT} is a proper reference to establish a reference in this framework. Indeed, the proper parameter for plasticity during SPT is P_Y at t/100 not only for 304, else for Al and 6061. It must be pointed out that the selection of method t/100 as most suitable,

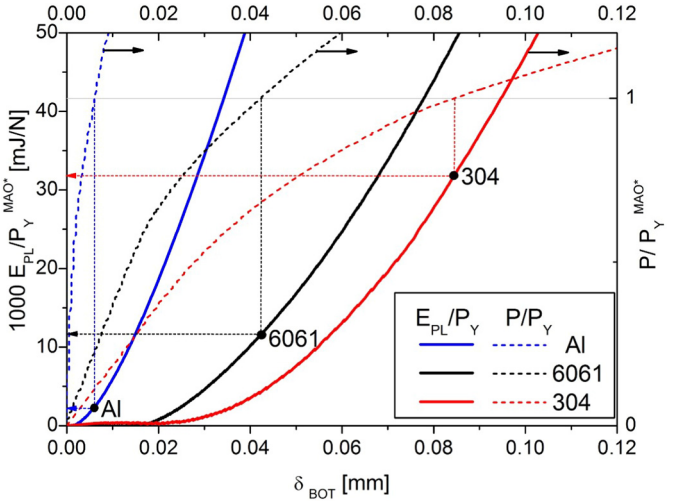

Fig. 10. Evolutions of normalized E_{PL}/P_Y (left axis) and load P/P_Y (right axis) for method Mao*.

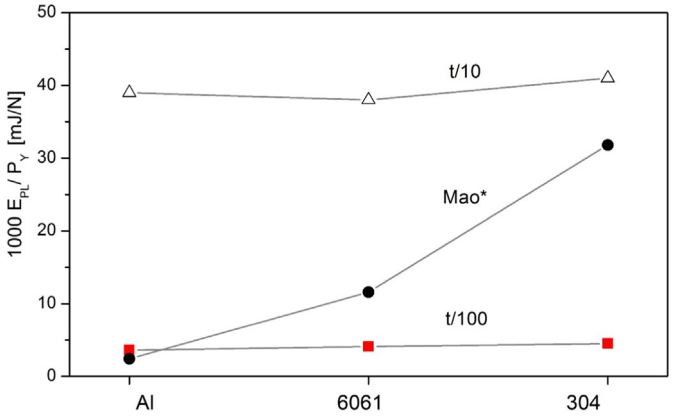

Fig. 12. Comparative results of normalized E_{PL} from Figs. 9, 10 and 11.

P_Y $^{t/100}$ represents the beginning of yielding spreading, previous to massive plastic deformation within regime II. As the consequence the correlation parameter $\alpha^{t/100}$ that predicts σ_{YS} has the strongest dependence of the material according the calculus for present work. Other methods Mao* and t/10 also showed such dependence in lower level. More extensive work is needed to make an approach for which parameters (microstructural for instance) could influence in this dependence.

Finally, the lower measurement of displacement δ_{BOT} resulted useful for this analysis to clarify the dependence E_{PL}. For that point of view it is strongly recommended use this displacement for further analysis of yielding to relate σ_{YS} as a function of P_Y or any parameters extracted from SPT plot.

4. Conclusions

The obtaining of yield stresses from characteristic load P_Y extracted from Small Punch Test was systematic studied in Al alloys and structural steels. From this study it can be concluded that:

The displacement measurements taken from the opposite side to contact ball (lower side of specimen and called δ_{BOT} in this work), is highly recommended due to directness of reading and more extended range lineal behavior of P vs. δ_{BOT} during the regime I. Both features were systematically tested for all materials tested in this work. This reading has the advantages of reflects mainly the Young modulus, due to delay to be influenced by plastic indentation. Also, there is no need to discount any displacement due to compliance of the load train. Finally, this methodology allows recognize the plastic spreading through the thickness from top to bottom specimen faces for a more clear definition of the characteristic load P_Y.

The application of semiempiric relationships between yield stress and P_Y/t^2 has been reviewed for four methods to calculate P_Y: Mao, Mao* t/100 and t/10. In this study Al alloys and structural steels were tested in disk-shaped specimens of 10 mm and 0.400, 0500 and 0.600 mm in thickness at room temperature.

The correlation parameters α obtained for the four methods Mao, Mao*, t/100 and t/10 showed different levels of dependence with materials. The assessment of yield strength by a single correlation parameter with high precision would be suitable for separated groups of materials but is not recommendable for a wide type of metallic materials. The highest difference between two parameters was for t/100 method where α $^{t/100}$ calculated for 6061 and Al was more than twice. Only 304, ADN and P91 steels gave α similar than that obtained by Mao, that is $\alpha^{M\alpha o} = 0.36$. For all materials of the present work the correlation parameter derived from P_Y ^{Mao} methodology resulted close similar to that obtained for $P_Y^{t/10}$.

The comparative analyzes of plastic energy taken from experimental plots were introduced as a criterion to establish a physics interpretation at P_Y in Al, 6061 and 304. The methodology t/100 offset was selected as the more representative of yielding due to both lowest values and the similar plastic energies obtained for three selected materials. In contrast for Mao* method there was a wide variation of energies and for t/10 method the values were much higher.

Acknowledgment

Thanks a lot to Mr. Jorge Bergaglio and Mr. Pablo Riquelme (Física de Metales, Centro Atómico Bariloche, Argentina) for technical assistance.

In memorial of Carlos "Popi" Gomez technical staff of Centro Atómico Bariloche, Argentina.

References

[1] S. Rasche, M. Kuna, Improved small punch testing and parameter identification of ductile to brittle materials, Int. J. Press. Vessel. Pip. 125 (2015) 23–34.
[2] S. Yang, X. Ling, Y. Zheng, Creep behaviors evaluation of Incoloy800H by small punch creep test, Mater. Sci. Eng. A 685 (2017) 1–6.
[3] M. Moreno, G. Bertolino, A. Yawny, The significance of specimen displacement definition on the mechanical properties derived from Small Punch Test, Mater. Des. 95 (2016) 623–631.
[4] T.E. García, C. Rodríguez, F.J. Belzunce, C. Suárez, Estimation of the mechanical properties of metallic materials by means of the small punch test, J. Alloys Compd. 582 (2014) 708–717.
[5] M. Coleman, H. Alshehri, R. Banik, W. Harrison, S. Birosca, Deformation mechanisms of IN713C nickel based superalloy during Small Punch Testing, Mater. Sci. Eng. A 650 (2016) 422–431, https://doi.org/10.1016/j.msea.2015.10.056.
[6] I.I. Cuesta, J.M. Alegre, M. Lorenzo, Influence of strain state in mechanical behaviour of aluminium alloys using the Small Punch Test, Mater. Des. 54 (2014) 291–294, https://doi.org/10.1016/j.matdes.2013.08.038.
[7] J. Alegre, I. Cuesta, M. Lorenzo, An extension of the Monkman-Grant model for the prediction of the creep rupture time using small punch tests, Exp. Mech. 54 (2014) 1441–1451, https://doi.org/10.1007/s11340-014-9927-6.
[8] A. Janča, J. Siegl, P. Haušild, Small punch test evaluation methods for material characterization, J. Nucl. Mater. 481 (2016) 201–213.
[9] K. Matocha, The use of small punch tests for determination of fracture behaviour of ferritic steels, Process. Eng. 86 (2014) 885–891, https://doi.org/10.1016/j.proeng.2014.11.110.
[10] CEN Workshop Agreement, CWA 15627:2006 E. Small Punch Test Method for Metallic Materials, CEN, Brussels, 2007.
[11] S. Jitsukawa, M. Kizaki, A. Umino, K. Shiba, A. Hishinuma, in: W.R. Corwin, E.M. Haggag, W.L. Server (Eds.), Methods and Devices for Small Specimen Testing at the Japan Atomic Energy Research Institute, Small Specimen Test Techniques Applied to Nuclear Reactor Vessel Thermal Annealing and Plant Life Extension, ASTM STP 1204, American Society for Testing and Materials, Philadelphia 1993, pp. 289–307.
[12] R.P. Harrison, D.G. Carr, T. Wei, P.A. Stathers, Materials surveillance program for the opal research reactor, Transactions 11th International Topical Meeting Research Reactor Fuel Management (RRFM) and Meeting Of The International Group On Reactor Research (IGORR) Centre De Congrès, Lyon, France, March 11–15 2007.
[13] M. Madia, S. Foletti, G. Torsello, A. Cammi, On the applicability of the small punch test to the characterization of the 1CrMoV aged steel: mechanical testing and numerical analysis, Eng. Fail. Anal. 34 (2013) 189–203.
[14] J.-Y. Jeon, Y.-J. Kim, S.-Y. Lee, J.-W. Kim, Extracting ductile fracture toughness from small punch test data using numerical modeling, Int. J. Press. Vessel. Pip. 139–140 (2016) 204–219.
[15] D. Andrés, R. Lacalle, J.A. Álvarez, Creep property evaluation of light alloys by means of the Small Punch test: creep master curves, Mater. Des. 96 (2016) 122–130.
[16] P. Dymáček, M. Jarý, F. Dobeš, L. Kloc, Tensile and creep testing of Sanicro 25 using miniature specimens, Materials 11 (1) (2018) 142, https://doi.org/10.3390/ma11010142.
[17] J.C. Chica, P.M. Bravo Díez, M.P. Calzada, Improved correlation for elastic modulus prediction of metallic materials in the Small Punch Test, Int. J. Mech. Sci. 134 (2017) 112–122.
[18] K. Matocha, R. Hurst, Small punch testing - the transition from a code of practice to a European testing standard, Key Eng. Mater. 734 (2017) 3–22, https://doi.org/10.4028/www.scientific.net/KEM.734.3.
[19] M.F. Moreno, Application of small punch testing on the mechanical and microstructural characterizations of P91 steel at room temperature, Int. J. Press. Vessel. Pip. 142–143 (2016) 1–9, https://doi.org/10.1016/j.ijpvp.2016.04.002.
[20] X. Mao, H. Takahashi, Development of a further-miniaturized specimen of 3 mm diameter for TEM disk (ϕ 3 mm) small punch tests, J. Nucl. Mater. 150 (1987) 42–52, https://doi.org/10.1016/00223115(1987)90092-4.
[21] D. Finarelli, M. Roedig, F. Carsughi, Small punch tests on austenitic and martensitic steels irradiated in a spallation environment with 530 MeV protons, J. Nucl. Mater. 328 (2004) 146–150.
[22] M. Eskner, R. Sandstrom, Mechanical property evaluation using the small punch test, J. Test. Eval. 32 (4) (2004) 1–8.
[23] J.C. Chica, P.M. Bravo Díez, M. Preciado Calzada, Development of an improved prediction method for the yield strength of steel alloys in the Small Punch Test, Mater. Des. 148 (2018) 153–166, https://doi.org/10.1016/j.matdes.2018.03.064.
[24] R.C. Hurst, K. Matocha, Renaissance in the use of the small punch testing technique Proceedings of the ASME, Pressure Vessels and Piping Conference PVP2015 July 19–23, 2015, Massachusetts, USA, Boston, 2015.
[25] IRAM/IAS U500-528, Barras de acero conformadas de dureza natural para hormigón armado, 1979 49–54.
[26] A. Dlouhy, N. Merk, G. Eggeler, A microstructural study of creep in short fibre reinforced aluminium alloys, Acta Metall. Mater. 41 (1993) 3245.
[27] M. Song, K. Guan, W. Qin, J.A. Szpunar, J. Chen, Size effect criteria on the small punch test for AISI 316L austenitic stainless steel, Mater. Sci. Eng. A 606 (2014) 346–353, https://doi.org/10.1016/j.msea.2014.03.098.
[28] E. Altstadt, M. Houska, I. Simonovski, M. Bruchhausen, S. Holmström, R. Lacalle, On the estimation of ultimate tensile stress from small punch testing, Int. J. Mech. Sci. 136 (2018) 85–93, https://doi.org/10.1016/j.ijmecsci.2017.12.016.
[29] H. Li, F.C. Chen, A.J. Ardell, A simple versatile miniaturized disk – bend test apparatus for quantitative yield – stress measurements, Metall. Trans. A. 22A (1991) 2061–2068, https://doi.org/10.1007/BF02669873.
[30] S. Haroush, E. Priel, D. Moreno, A. Busiba, I. Silverman, A. Turgeman, R. Shneck, Y. Gelbstein, Evaluation of the mechanical properties of SS-316L thin foils by small punch testing and finite element analysis, Mater. Des. 83 (2015) 75–84.